Blade cooling optimisation in humid-air and steam-injected gas turbines

J.P.E. Cleeton, R.M. Kavanagh, G.T. Parks

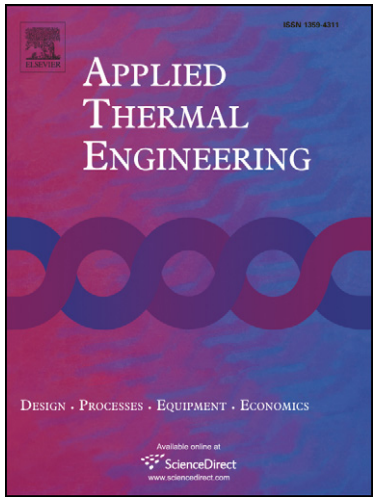

Blade cooling optimisation in humid-air and steam-injected gas turbines

J.P.E. Cleeton, R.M. Kavanagh, G.T. Parks

PII: S1359-4311(09)00134-3
DOI: 10.1016/j.applthermaleng.2009.04.034
Reference: ATE 2793

To appear in: *Applied Thermal Engineering*

Received Date: 17 August 2008
Revised Date: 1 April 2009
Accepted Date: 10 April 2009

Please cite this article as: J.P.E. Cleeton, R.M. Kavanagh, G.T. Parks, Blade cooling optimisation in humid-air and steam-injected gas turbines, *Applied Thermal Engineering* (2009), doi: 10.1016/j.applthermaleng.2009.04.034

BLADE COOLING OPTIMISATION IN HUMID-AIR AND STEAM-INJECTED GAS TURBINES

J. P. E. Cleeton *, R. M. Kavanagh, G. T. Parks

Department of Engineering

University of Cambridge

Trumpington Street

Cambridge, CB2 1PZ, UK

Abstract

Humidified gas turbine cycles such as the Humidified Air Turbine (HAT) and the Steam-Injected Gas Turbine (STIG) present exciting new prospects for industrial gas turbine technology, potentially offering greatly increased work outputs and cycle efficiencies at moderate costs. The availability of humidified air or steam in such cycles also presents new opportunities in blade and disk cooling architecture. Here, the blade cooling optimisation of a HAT cycle and a STIG cycle is considered, first by optimising the choice of coolant bleeds for a reference cycle, then by a full parametric optimisation of the cycle to consider a range of optimised designs. It was found that the coolant demand reductions which can be achieved in the HAT cycle using humidified or post-aftercooled coolant are compromised by the increase in the required compression work. Furthermore, full parametric optimisation showed that higher water flow-rates were required to prevent boiling within the system. This

corresponded to higher work outputs, but lower cycle efficiencies. When optimising the choice of coolant bleeds in the STIG cycle, it was found that bleeding steam for cooling purposes reduced the steam available for power augmentation and thus compromised work output, but that this could largely be overcome by reducing the steam superheat to give useful cycle efficiency gains.

Key words: Blade cooling, humid cycles, steam injection, optimisation, gas turbine

1 Introduction

Humidified power cycles present one of the key areas of development within the gas turbine industry. Cycles such as the Humidified Air Turbine (HAT) or the Steam-Injected Gas Turbine (STIG) promise work outputs and cycle efficiencies comparable to those of a Combined-Cycle Gas Turbine, but at a capital cost more comparable to a conventional gas turbine cycle. Gas turbines such as the GE LM2500 STIG have started to be used commercially [1], but the HAT cycle remains at the pilot plant stage, with the 600 kW_e Volvo VT600 derivative at Lund University being the first working pilot plant [2]. Such cycles also present the opportunity for new blade and disk cooling architectures, whereby humidified air or steam, coolants with higher specific heat capacities than air, may be used in turbine blade and disk cooling, currently one of the limiting factors in optimising gas turbine performance.

In the first part of this investigation, the coolant bleed configuration within feasible HAT and STIG cycle layouts is optimised with respect to cycle efficiency, and the effects and consequences of bleeding coolant from the saturator,

* Corresponding author. Fax:+44 (0)1223 3 32662; Email: jpec2@cam.ac.uk

in the case of the HAT cycle, or the Heat Recovery Steam Generator (HRSG) and steam/air mixer for the STIG cycle are considered. The remaining cycle parameters were fixed: the coolant bleed points are the only variables considered. It is important to differentiate between the optimal thermodynamic configuration and a practical configuration: both were investigated. In the optimal thermodynamic configuration no constraint was placed on the number of coolant bleeds that could be used, but for the practical configuration, where cost and complexity must necessarily be considered, the number of bleeds was restricted to three, which is typical of an industrial gas turbine.

In the second half of the investigation, Pareto-optimal sets of designs for the HAT and STIG cycles were produced, and a Tabu Search (TS) algorithm, developed by Jaeggi et al. [3] and implemented on humid cycles by Kavanagh [4], was used to carry out a parametric optimisation of the cycles. The humidified cycle output parameters were calculated using FORTRAN code developed by Aramayo-Prudencio [5] and Kavanagh in the University of Cambridge Department of Engineering, based on code developed for standard industrial gas turbine cycles by Young and Wilcock [6], in the same department. All of the cycles discussed consisted of two stages (or four blade rows) of blade cooling, and three stages of disk cooling. However, since it is very difficult to model disk cooling accurately, the disk cooling flows are pre-determined, with the focus in this investigation being placed on turbine blade cooling.

NOMENCLATURE

A_g	Blade throat area (m^2)
A_{ij}	Mason and Saxena modification factor
A_{surf}	Total external blade surface area (m^2)

c_p	Specific heat capacity at constant pressure (kJ/kg K)
f	Vector of objective functions
K_{cool}	Dimensionless cooling flow factor
M	Molar mass (kg/kmol)
m	Mass flow-rate (kg/s)
N	Number of design variables
n	Number of mainstream gas constituents
Nu	Nusselt number
Pr	Prandtl number
Re	Reynolds number
r_p	Pressure ratio
St	Stanton number
T	Temperature (K)
x	Vector of design variables
y	Mole fraction
λ	Thermal conductivity (W/m K)
μ	Dynamic viscosity (kg/m s)
ω	Specific humidity (kg_v/kg_{tot})
η_{ov}	Overall efficiency (%)

Abbreviations

AC	Aftercooler
ECO	Economiser
FPT	Free-Power Turbine
H&J	Hooke and Jeeves
HAT	Humidified Air Turbine

HP	High Pressure
HRSG	Heat Recovery Steam Generator
IC	Intercooler
IM	Intensification Memory
IP	Intermediate Pressure
LP	Low Pressure
LTM	Long Term Memory
MTM	Medium Term Memory
REC	Recuperator
SAT	Saturator
ST	Steam from the HRSG
STM	Short Term Memory
STIG	Steam-Injected Gas Turbine
SA	Steam/Air Mixture
TBC	Thermal Barrier Coating
TS	Tabu Search

Subscripts

aw	Adiabatic blade wall
c	Coolant
g	Mainstream gas
i	Inlet
w	Blade wall
x	Exit
0	Stagnation property

2 Analysis and Optimisation Methods

2.1 The Blade Cooling Model

The blade cooling model used is that used by Wilcock [7], shown in Fig 1: variations of the model may be valid for other applications where film cooling is utilised. Coolant bled at state k is transported to the blade cooling passages, entering the blade at state i (assumed to be identical to k). When only convective cooling is used, the coolant leaves the blade at the trailing edge and tip at states t and b respectively. When film cooling is also considered, some coolant leaves the blade through various holes across the blade surface, where the coolant is assumed to be at state f everywhere, and at the endwalls at state e. An extended Holland and Thake model [8], as used by Young and Wilcock [6], is then used to carry out an enthalpy balance between the coolant and mainstream gas, which is equal to the total blade surface heat transfer. This is also equal to the heat transfer via conduction through the blade metal, and any thermal barrier coating.

[Fig. 1 about here.]

The coolant mass flow-rate with respect to the compressor inlet mass flow-rate (m_c/m_g) can be defined in terms of a dimensionless coefficient K_{cool}, and a dimensionless coolant mass flow-rate m_{c+} as follows:

$$m_c/m_g = K_{cool} m_{c+} \tag{1}$$

where

$$K_{cool} = \frac{A_{surf}}{A_g}\frac{c_{p,g}}{c_{p,c}}St \tag{2}$$

$$m_{c+} = \frac{T_{aw} - T_w}{T_{0c,x} - T_{0c,i}} \tag{3}$$

The value of K_{cool} is therefore proportional to the mainstream Stanton number, which is itself based on an empirical relationship with the gas Reynolds and Prandtl numbers given by Torbidoni and Horlock [9]:

$$St_g = 0.285 Re_g^{-0.37} Pr_g^{-2/3} \tag{4}$$

K_{cool} is also inversely proportional to the coolant specific heat capacity, indicating that a coolant with a higher c_p will reduce coolant mass flow-rate, as one might expect. m_{c+} meanwhile is dependent on the efficiencies of the cooling technology, and on blade material and geometry (and is consequently of less interest for this investigation). Hence the key to minimising cooling demands is minimising K_{cool}.

The focus of this investigation will be blade cooling and not disk cooling. This is because disk cooling flows are very difficult to calculate accurately: wherever disk cooling is necessary, the disk coolant mass flow-rates (relative to the turbine flow-rate) will be pre-specified. This is consistent with the work of Wilcock [7].

The coolant performance is, through the Stanton number, strongly dependent on the mainstream gas Reynolds and Prandtl numbers, as indicated in Eq. (4). The mainstream gas properties are dependent on the properties of the individual constituents. Thus the mainstream gas thermal conductivity λ_g was found using the Wassiljewa model [10] with the Mason and Saxena modification [11],

as investigated by Todd and Young [12], which considers the molar fractions of the various constituents of the gas:

$$\lambda_g = \sum_{i=1}^{n} \frac{y_i \lambda_i}{\sum_{j=1}^{n} y_i A_{ij}} \tag{5}$$

where y_i and λ_i are the mole fraction and thermal conductivity of component i respectively, and A_{ij} is found from the Mason and Saxena modification [11]:

$$A_{ij} = \frac{(1 + (\mu_i/\mu_j)^{0.25})^2}{(8(1 + M_j/M_i))^{0.5}} \tag{6}$$

where μ_i and M_i are the dynamic viscosity and molar mass of component i respectively. Bird, Stewart and Lightfoot [13] demonstrate how the mainstream gas dynamic viscosity μ_g can be calculated in an identical fashion, replacing λ_i with μ_i.

2.2 Tabu Search Optimiser

The numerical optimiser used in this study is a variant of the multi-objective Tabu Search (TS) algorithm developed by Jaeggi et al. [3].

We are interested in problems where multiple objective functions are each to be minimised (noting that the maximum of objective f is the minimum of $-f$). When true multi-objective design optimisation is performed the solution is a set of designs representing the optimal set of trade-offs between the objectives. This is known as the *Pareto-optimal* set. This set provides the designer with a clear picture of the achievable trade-offs between the competing objectives, enabling a well-informed choice of final solution to be made.

Solutions in the set are said to be *Pareto equivalent* to each other and non-dominated by any other solution. If f_n is the vector of objective function values

for design point x_n, x_n is said to be Pareto equivalent to another point x_m if some components of f_n are larger than the corresponding components of f_m while other components of f_n are smaller than the corresponding components of f_m. Similarly, x_n *dominates* x_m if all components of f_n are less than or equal to the corresponding components of f_m and at least one component is less.

TS explores the available search space through local search using rules that temporarily exclude some search points from consideration (making points "tabu") to overcome difficulties, such as local optimum trapping. It operates in a sequential, iterative manner: the search starts at a given point and the algorithm selects a new point in the search space to be the next current point. The basic search pattern in this implementation is a modified version of Hooke and Jeeves (H&J) search [14]. Allowing for points that violate constraints or are tabu (see below), the H&J local search strategy requires approximately $2N$ solution evaluations, where N is the number of design variables.

A real-world problem may contain a large number of design variables and this strategy can become prohibitively expensive. The solution adopted is to incorporate an element of random sampling in the H&J step. The $2N$ new points are generated, those that are tabu or infeasible are removed, and only $n_{sample} \leq 2N$ points from those that remain are evaluated, selecting randomly to avoid introducing any directional bias. If one of these points dominates the current point, it is automatically accepted as the next point. If more than one point dominates the current point, a non-dominated point from these is randomly selected. If no points dominate the current point, a further n_{sample} points are sampled and the comparison is repeated. If all the feasible, non-tabu points have been sampled without finding a point that dominates the current solution, the standard selection procedure is employed.

Recently visited points are stored in the *Short Term Memory* (STM) on a first-in-first-out basis and are *tabu* – the search is not allowed to revisit these points.

The *Medium Term Memory* (MTM) maintains a record of the Pareto-optimal points found thus far during search, and its contents are the primary output at the end of the optimisation.

[Table 1 about here.]

An *Intensification Memory* (IM) stores locally Pareto-optimal points that have not been selected as part of the H&J search pattern; the IM is used to select points for *search intensification*, focusing the search on areas of the search space with known good objective function values. The *Long Term Memory* (LTM) records the regions of the search space which have been explored, and is used on *diversification*, directing the search to regions which are under-explored. This is achieved by dividing the allowed range for each design variable into a certain number of regions and counting the number of solutions evaluated in those regions. A local iteration counter i_{local} is used, and reset upon a successful addition to the MTM. When i_{local} reaches user-specified values, the algorithm will diversify or intensify the search, or reduce the search step-size and restart the search from a randomly selected point from the MTM. Thus, TS combines a systematic local search with a stochastic element and an intelligent coverage of the entire search space. Full details of this algorithm can be found in [3], and the optimiser parameters used in this research are summarised in table 1.

3 Cycle Layouts

The HAT cycle (shown in Fig. 2) turbine consists of an HP and an IP stage, with an additional free-power turbine (FPT). The values of the pressure ratios r_p for the HP and IP stages are constrained by the required compression work, with the FPT expanding to atmospheric pressure. In addition to the simple gas turbine core are the saturator, intercooler, aftercooler and recuperator. As it is necessary to heat the water entering the saturator, the exergy losses of the flue gases are greatly reduced by the inclusion of an economiser to heat the water, and reduced further still by including a recuperator to raise the temperature of the saturated air before it enters the combustor. The water temperature is increased further by the use of an intercooler and aftercooler, with the intercooler having the advantage of lowering the required compressor work. The various coolant bleed points and the points of coolant delivery are also shown in Fig. 2. Note that the numbers following HP, IP and LP refer to the stage in the case of a compressor, but to the blade row in the case of a turbine. Coolant bled from a compressor stage is always taken at the stage exit condition.

[Fig. 2 about here.]

The layout of the STIG cycle model is shown in Fig. 3, complete with coolant bleed and delivery locations. The core gas turbine layout and component characteristics are identical to the HAT cycle, with the obvious addition of a Heat Recovery Steam Generator (HRSG) to generate steam, and a mixer for the steam and compressed air. The cycle parameters, shared by both the HAT and STIG cycles, are given in table 10 in Appendix 1, whilst parameters specific

to the HAT and STIG cycles are shown in table 11, also in Appendix 1.

[Fig. 3 about here.]

For both the HAT and STIG cycles, coolant delivery pressure to mainstream gas pressure ratios of 1 to 1.5 were permitted: note that a pressure ratio of 1 presents an absolute limit which could not be achieved in practice. The minimum pinch point temperature difference across the various heat exchangers was 10K, as was the maximum allowable difference between the water temperature and its boiling temperature in the case of the HAT cycle. As a result it was necessary in some cases to slightly reduce heat exchanger effectiveness for some of the HAT configurations, in order to reduce the water temperature.

3.1 Cooling Optimisation for a Fixed Parameter System

3.1.1 HAT Cycle Coolant Bleed Layout

The analysis considered both realistically achievable layouts, with a maximum constraint on number of bleed points, and fully optimised cycles, with no limit to the number of bleed points. It was also important that a direct comparison could be made between fully dry air-cooled cycles and cycles which implement humidified air-cooling. Hence the following 4 layout specifications were chosen:

A Dry air-cooled, fully optimised

B Dry air-cooled, optimised with a maximum of 3 different bleed points

C First two blade rows cooled with humidified air, fully optimised

D First two blade rows cooled with humidified air, optimised with a maximum of 3 different bleed points

In cases C and D, the humidified air was supplied from the saturator exit. Note that the cycles have been optimised to maximise overall efficiency, *not* necessarily to minimise cooling demands.

3.1.2 STIG Cycle Coolant Bleed Layout

As with the HAT cycle, both fully optimised and realistically optimised (a maximum of 3 bleed points) configurations were considered. The STIG cycle offers the opportunity to bleed pure steam from the HRSG exit, or a steam/air mixture once the steam and air streams have been mixed: both options have been considered here. All sources of steam-cooling were performed as open loop. The following cases were considered for the arrangement of coolant bleeds:

A Dry air-cooled, fully optimised

B Dry air-cooled, optimised with a maximum of 3 different bleed points

HRSG Steam Cases:

C First two blade rows cooled with steam, fully optimised

D First two blade rows cooled with steam, optimised with a maximum of 3 different bleed points

E All blade rows cooled with steam

Steam/Air Mixture Cases:

F First two blade rows cooled with steam/air mixture, fully optimised

G First two blade rows cooled with steam/air mixture, optimised with a maximum of 3 different bleed points

A large fraction of the steam may be used for purposes other than power augmentation (process steam). Steam was bled from the HRSG before the re-

maining steam was split into two separate streams: a mixer stream for power augmentation, and a stream for process steam. Two possibilities were considered: one where 50% of the steam leaving the HRSG (after coolant has been bled) was process steam, and one where 100% of the steam was used for power augmentation.

4 Results and Discussion

4.1 Cooling Optimisation for a Fixed-Parameter Cycle

4.1.1 HAT Cycle Results

The coolant bleed configurations for the various HAT cases as a result of optimistion are given in table 2 using the same notation shown in Fig. 2, whilst table 3 considers the overall cycle performance for the four cases. It is evident that significant coolant demand reductions (around 12%, relative to case A) have been achieved by bleeding from the saturator. Usefully, reducing the number of bleed points to three in case D has had no detrimental effect on cooling performance. It is important to understand, however, that the coolant being bled after the saturator is at a much lower temperature than the original bleed point after the HP compressor. The saturator exit temperature was almost identical for all cases, and averaged around 422.5K, whilst the temperature at HP compressor exit was around 591K. It was estimated that no more than 20% of the savings were contributed by the elevated ω_c, and that the remaining savings were due to a reduced coolant temperature.

[Table 2 about here.]

[Table 3 about here.]

Comparing the fully optimised cycles A and C shows that the inclusion of humid air-cooling for C results in an improved net work output, but a reduced η_{ov}. Reducing cooling demands has increased mass flow into the turbine, but by bleeding post-saturator the air must now be fully compressed before it can be bled off for cooling. Consequently, r_p (and the net work output) of the FPT for case C has only been slightly increased from case A, whilst the increased mass flow into the combustion chamber also increases the heat input required, reducing η_{ov}. The problem would be exacerbated by cooling additional downstream blade rows with humidified air – hence the reason this analysis was restricted to the first two rows only. Comparing the realistically optimised cycles B and D yields more promising results: the overall efficiencies were almost identical, with a 1.5 %-point increase in net work output from B to D. By reducing complexity of the coolant architectures to a more realistic level, the net benefits of bleeding coolant post-saturator have been greatly increased.

4.1.2 STIG Cycle Results

The coolant bleed configurations for both 50% and 100% steam utilisation are shown in tables 4 and 5 respectively, using the same notation shown in Fig. 3, whilst tables 6 and 7 give the performance figures for all cases for the 50% and 100% steam utilisation scenarios respectively.

When considering 50% of the steam being delivered to the mixer, for cases C and D, the use of steam for the first row reduced coolant demands for that row by almost 55%, and a saving of almost 38% was made for row 2. Cooling all of the rows with steam (case E) yields further overall improvement. Steam/air

mixture cooling (cases F and G), due to its higher temperature and lower c_p, relative to the pure steam, did not perform nearly so well, indeed, performing worse than dry air-cooling.

Similar observations are made for the scenario where all of the produced steam enters the cycle: the increased quantity of steam within the cycle raises cooling demands for all cases, but the relative savings which can be made by steam-cooling are in fact greater. Note that any steam bled for cooling purposes bypasses the combustion chamber: the reduced c_{pg} alleviates cooling demands, relative to the case where the turbine is fully air-cooled, and therefore when more steam is injected into the mixer.

[Table 4 about here.]

[Table 5 about here.]

When 50% of the generated steam is taken to the steam/air mixer, the steam used for cooling, which is later mixed with the mainstream gas, is "free" steam. The mass flow entering the first turbine is significantly increased by steam cooling, resulting in a significant work output gain, which is only partially compromised by a slight rise in HP compression work. This resulted in more than a 1.3 %-point improvement in η_{ov} for case C. Limiting the number of bleed points to three, as in case D, only cost a 0.1 %-point penalty. Cooling the remaining blade rows with steam (case E) brought further small improvements to the net work output and η_{ov}. However, cooling with a steam/air mixture reduced η_{ov} (and even the net work output) due to the increased compression work.

When 100% of the generated steam is injected into the cycle, any steam which

is used as coolant bypasses the combustion chamber: this reduces c_{pg} of the flow leaving the combustion chamber which, whilst lowering the subsequent coolant demands, also implies a larger temperature (and hence pressure) drop across the HP and IP turbines to carry out the required compression work. The value of r_p across the FPT is thus reduced, and the net work output is actually below what can be achieved with dry air-cooling. Nonetheless, a small improvement in η_{ov} has been achieved, due to the reduction in heat input required in the combustion chamber. This is for steam cooling only: steam/air mixture cooling results in a reduction in η_{ov} and net work output for the reasons given earlier.

[Table 6 about here.]

[Table 7 about here.]

4.2 Cooling Optimisation with Parameter Optimisation

4.2.1 HAT Cycle Cooling Optimisation

A multi-objective TS optimisation of the efficiency and work output of the HAT cycle, subject to the bounds and constraints set by Kavanagh and Parks [15], yielded 145 designs, of which three were selected for subsequent cooling optimisation, as shown in Fig. 4. Optimising the cooling architecture separately from the other system parameters proved challenging, since the optimised parameters for these designs lay very close to the system constraints. One of two constraints was met: either water approached its boiling point, or the pressure of the coolant source was too low to be utilised. It therefore proved impossible to bleed any coolant from either the saturator exit or the

aftercooler exit for the three designs considered, and the improvements in both cooling and efficiency, relative to the reference case, are shown in table 8 to be only marginal.

[Fig. 4 about here.]

When the cooling architecture was included as an additional design variable in the optimisation, the resulting Pareto-optimal set was able to make 0.3-0.5 %-point efficiency gains, and significant coolant savings. Whilst the coolant for turbine blade rows HP2, IP1 and IP2 was always taken from compressor stages HP4, HP3 and HP1 respectively across the entire Pareto-optimal set, the optimal bleed point for turbine stage HP1 varied depending on the design location within the set. For high efficiency systems, compressor stage HP5 was chosen, whilst for low efficiency but high work output systems, the coolant was bled post-saturator or post-aftercooler. This variation in bleed point across the Pareto-optimal set is due to the balance struck between reducing cooling demands and minimising the water flow-rate in the system. Bleeding post-saturator or post-aftercooler rather than from the compressor tended to cause water to boil in the system. This is because the mass flow of cool gas into the recuperator is reduced, thereby increasing the temperature of the hot gas entering the economiser, causing water to boil in the system. Thus, a larger water flow-rate is required to move away from this constrained region, which in turn reduces efficiency. When bleeding coolant from the compressor (i.e. before the aftercooler) the gas flow through the aftercooler is also reduced, and so boiling is less likely to occur.

[Table 8 about here.]

To confirm the effects of this constraint, a set of Pareto-optimal designs were found where the coolant bleeds were constrained to be post-saturator and post-aftercooler only. Fig. 5 shows that the resulting designs were unable to improve upon the overall efficiencies achieved by the Pareto-optimal set with optimised cooling (Original Pareto 1). Note also the improved performance of the optimised cooling architecture Pareto-optimal compared to the original HAT Pareto-optimal set as shown in Fig. 6.

[Fig. 5 about here.]

[Fig. 6 about here.]

4.2.2 STIG Cycle Cooling Optimisation

As with the HAT cycle, a Pareto-optimal set was found for the reference STIG cycle, again subject to the bounds and constraints set by Kavanagh and Parks [15], from which three designs (shown in Fig. 7) were chosen for the parametric optimisation algorithm. Steam utilisation was 100% for all designs. For Design 1 it was impossible to use either steam or a steam/air mixture for cooling, since it resulted in the minimum approach temperature constraint (the temperature difference between the exhaust gas entering and the steam leaving the HRSG) being exceeded. By bleeding steam as coolant, the steam injection flow-rate is reduced, and, for a fixed pressure ratio, this results in a larger temperature ratio across the turbine, consequently reducing the exhaust temperature. The approach temperature was larger for Design 2, so steam or steam/air could be used, but the high steam temperature (787K compared to 739K when bleeding from HP6), coupled with the reduced steam injection flow-rate into the turbine, meant that there was no benefit from doing

this. Only for Design 3, where the approach temperature was larger still, was bleeding from the steam/air mixture beneficial. The findings here are thus consistent with the simple cooling optimisation carried out previously.

[Fig. 7 about here.]

When the multi-objective TS algorithm was applied to the Pareto-optimal set, significant benefits (0.3-0.5 %-points) were seen in efficiency, in addition to 15-35% reductions in coolant, as shown in table 9. The bleed points for the IP turbine stator and rotor remained unchanged throughout, but cooling of the HP turbine stator and rotor was achieved by steam or steam/air cooling for all but the lowest efficiency (but highest work output) designs, where compressor stage HP6 remained as the bleed point. Earlier it was seen that only marginal efficiency gains were achieved by a simple coolant bleed optimisation, but when the whole system is optimised, much higher gains with steam or steam/air can be achieved, as illustrated in Fig. 8.

[Table 9 about here.]

[Fig. 8 about here.]

The most obvious parameter change was the degree of superheat applied (see Fig. 9). Typically, high superheats favour high efficiencies, whilst low superheats favour higher steam-injection rates and thus higher work outputs. However, increasing superheat will also increase the blade cooling requirements: if steam is to be used for cooling, then its benefits as a coolant must outweigh the subsequent reduction in steam-injection. However, lower superheats were now found to favour higher efficiency, and the superheats were being reduced from 210-265K to 185-210K in Pareto-optimal designs found by the TS algo-

rithm. Reducing the superheat also permits higher pressure ratios, since less heat exchange is required in the HRSG, and so lower exhaust gas temperatures are possible. It should be noted that coolant for the IP turbine disk was bled from HP3 instead of LP6, due to coolant pressure constraints.

[Fig. 9 about here.]

5 Discussion

There are several limitations and extensions to this work which could provide interesting and fruitful areas of future research. Rather than taking a typical aero-derivative engine, a portfolio of different gas turbines could be investigated. Looking to the future, higher turbine inlet temperatures could be analysed as well as the potential cooling limitations, which are accentuated in humid cycles. In addition, other variants on the humid power systems (recuperated-STIG, intercooled-STIG, A-HAT, part-flow HAT) could also be studied using the methodology developed for this work. Further consideration also needs to be given to utilising these turbine cycles in applications with the co-generation of electricity and heat.

A more ambitious optimisation strategy may be required where configuration optimisation is undertaken. Rather than just optimising parameters, the optimiser would evolve the cycle configuration to generate the best performance. This might require a new optimisation strategy: although the TS algorithm was developed to allow handling of integer variables for the cooling system, evolving new system architectures may prove too challenging.

The cooling model was further developed over the course of this work but

further advances can still be made. Currently, open-loop steam cooling is simulated and research into closed-loop steam cooling still needs to be undertaken.

6 Conclusions

The cooling optimisation of a HAT cycle and a STIG cycle has been carried out, first by a simple coolant bleed optimisation of a reference cycle, then in conjunction with a multi-objective optimisation of the entire cycle. For the HAT cycle, it was found, in general, that bleeding post-aftercooler or post-saturator, whilst reducing coolant demands, had the undesirable effect of increasing compression work, resulting in only marginal efficiency gains. Furthermore, the multi-objective optimisation showed that bleeding from these locations was constrained by a tendency for water to boil within the system, and a need for larger water flow-rates to prevent this. Thus, these bleed points favoured low efficiency, high work output cycles, whilst the opposite is true for conventional compressor bleeding.

Both 50% and 100% steam utilisation were considered in the simple optimisation of the STIG cycle. For the 50% case, steam cooling yielded considerable improvements, since the steam used in cooling was "free" steam, and did not affect the steam-injection rate. This is not the case for 100% steam utilisation where steam bled for cooling compromises the work output, and so only marginal efficiency gains were seen. However, when carrying out a multi-objective optimisation of a STIG cycle with 100% steam utilisation, much larger (0.3-0.5 %-point) efficiency gains were achievable. This was largely due to a reduction in the optimal superheat temperature, which resulted in reduced overall cooling demands and enhanced benefits in using steam as a coolant, as

well as a higher permissible turbine pressure ratio.

It was noted that producing a Pareto-optimal set of designs and then performing a subsequent parametric optimisation did not yield the best results. When the cooling streams were included in the parameters for optimisation, much greater benefits were seen for both the HAT and the STIG cycles.

References

[1] Gas Turbine World 2001-2002 Handbook, 2001.

[2] T. Lindquist, P.M. Rosén, T. Torisson, Evaporative gas turbine cycle - a description of a pilot plant and operating experience, ASME, AES (40) (2000) 511-520.

[3] D.M. Jaeggi, G.T. Parks, T. Kipouros, P.J. Clarkson, The development of a multi-objective Tabu Search algorithm for continuous optimisation problems, European Journal of Operational Research 185 (3) (2008) 1192-1212.

[4] R.M. Kavanagh, Analysis and optimisation of humidified power cycles, PhD Thesis, University of Cambridge, 2008.

[5] A. Aramayo-Prudencio, Thermodynamics of water injected gas turbine cycles, PhD Thesis, University of Cambridge, 2004.

[6] J.B. Young, R.C. Wilcock, Modelling the air-cooled gas turbine part 2 – Coolant flows and losses, Journal of Turbomachinery 124 (2) (2002) 214-221.

[7] R.C. Wilcock, The thermodynamics of cooling in high temperature gas turbines, PhD Thesis, University of Cambridge, 2002.

[8] M.J. Holland, T.F. Thake, Rotor blade cooling in high-pressure turbines, Journal of Aircraft 17 (6) (1980) 412-418.

[9] L. Torbidoni, J.H. Horlock, A new method to calculate the coolant requirements of a high temperature gas turbine blade, Journal of Turbomachinery 127 (1) (2005) 191-199.

[10] A. Wassiljewa, Wärmeleitung in Gasgemischen, Physikalisches Zeitschrift 5 (22) (1904) 737-742.

[11] E.A. Mason, C.S. Saxena, Approximate formula for the thermal conductivity of gas mixtures, Physics of Fluids 1 (5) (1958) 361-369.

[12] B. Todd, J.B. Young, Thermodynamic and transport properties of gases for use in solid oxide fuel cell modelling, Journal of Power Sources 110 (1) (2002) 186-200.

[13] R.B. Bird, W.E. Stewart, E.N. Lightfoot, Transport Phenomena, 2nd Ed., John Wiley & Sons, New York, 2002.

[14] R. Hooke, T.A. Jeeves, 'Direct search' solution of numerical and statistical problems, Journal of the Association of Computing Machinery 8 (2) (1961) 212-229.

[15] R.M. Kavanagh, G.T.Parks, A systematic comparison and multi-objective optimisation of humid power cycles: Part 1 - Thermodynamics, ASME Turbo Expo (2008) GT2008-51508.

7 APPENDIX 1: CYCLE REFERENCE PARAMETERS

[Table 10 about here.]

[Table 11 about here.]

List of Figures

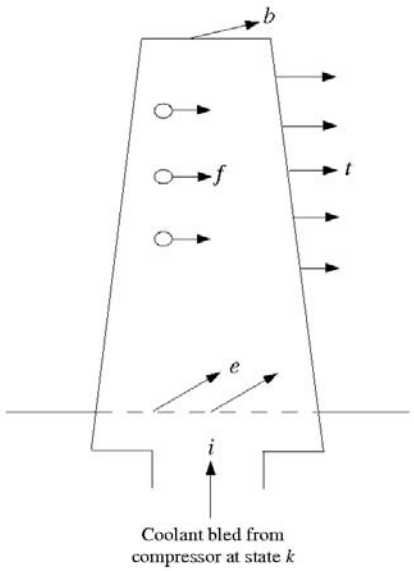

Fig. 1. Schematic diagram of a cooled turbine blade

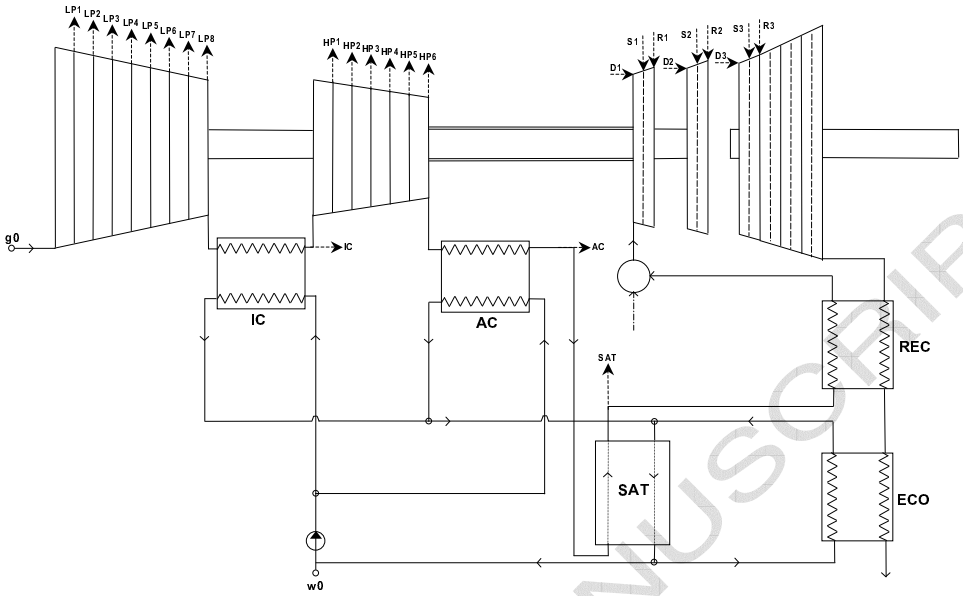

Fig. 2. The HAT cycle

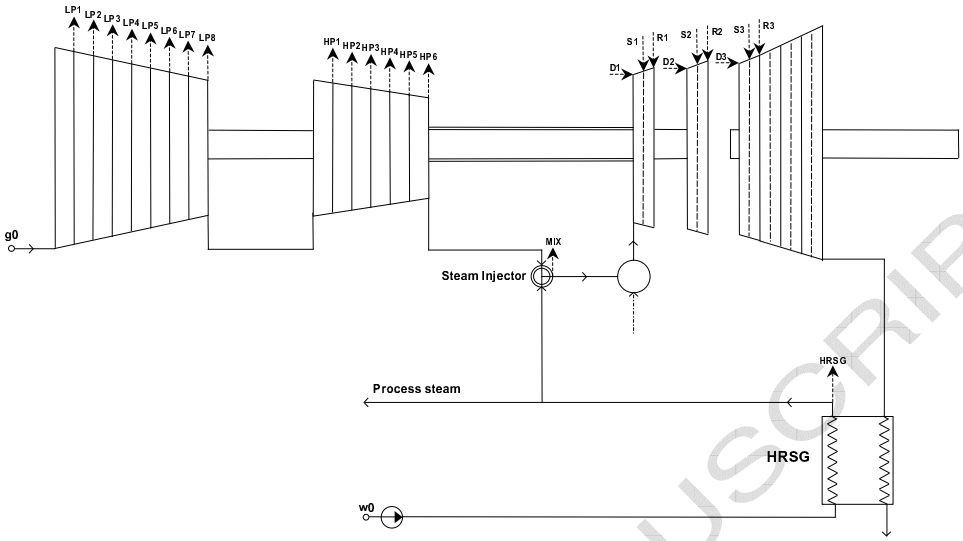

Fig. 3. The STIG cycle

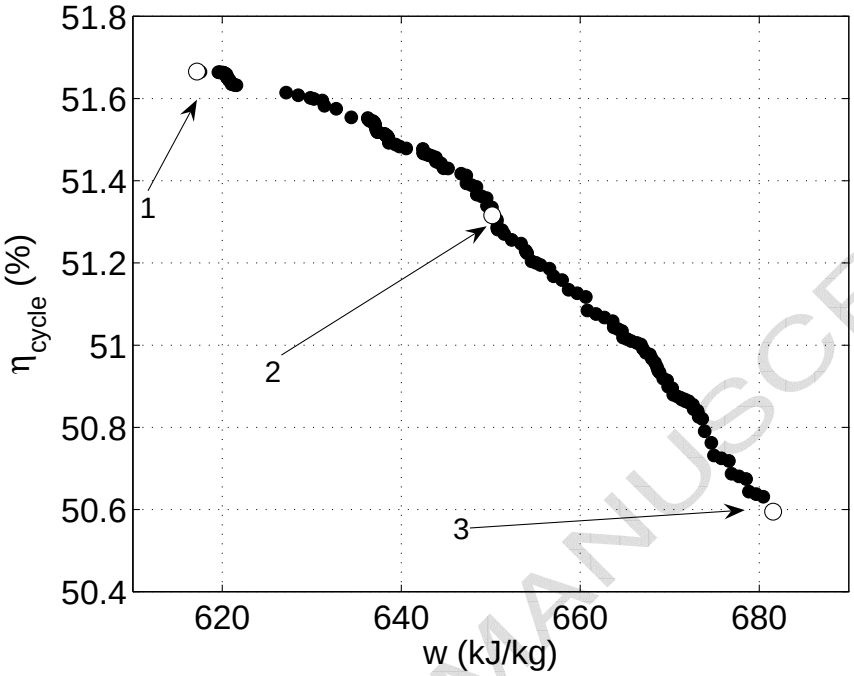

Fig. 4. Selected HAT systems from Pareto-optimal set for cooling optimisation

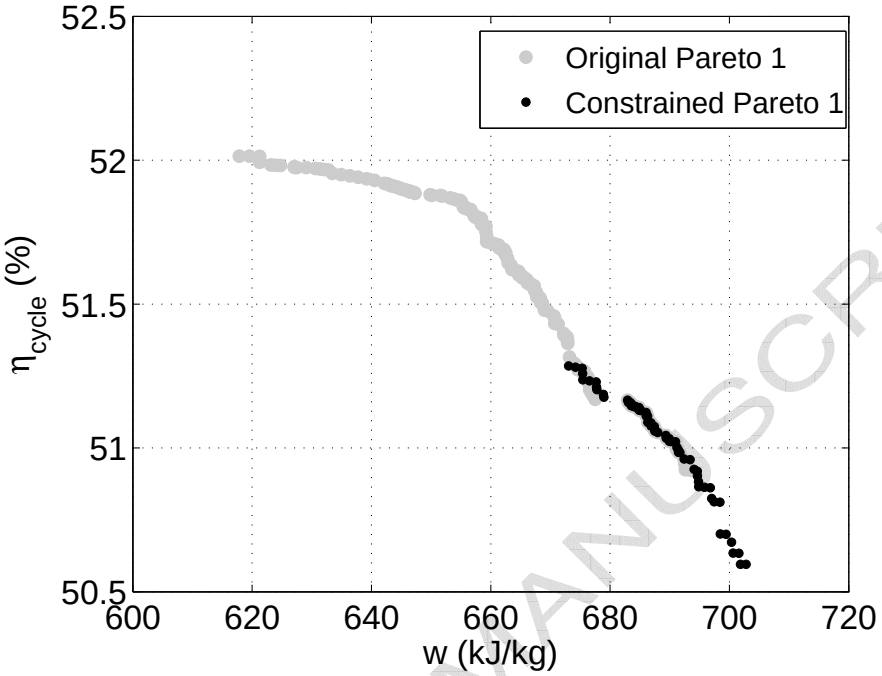

Fig. 5. Pareto-optimal sets for cooling optimised HAT cycles without and with cooling bleeds constrained to be post-saturator and post-aftercooler

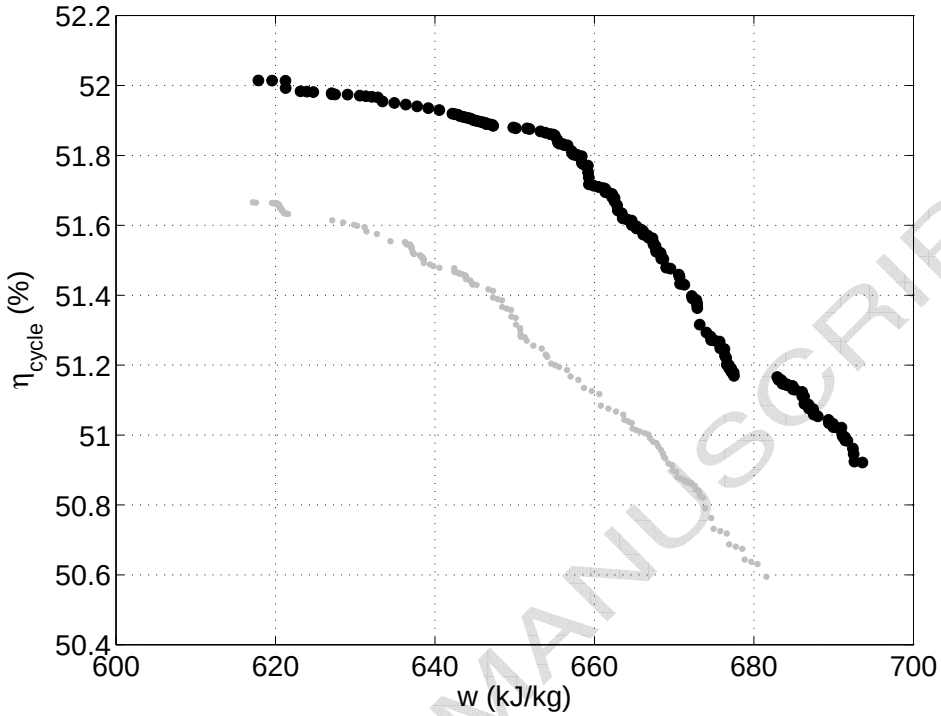

Fig. 6. Comparison of the cooling optimised HAT Pareto-optimal set (black dots) and the original Pareto-optimal set (gray dots)

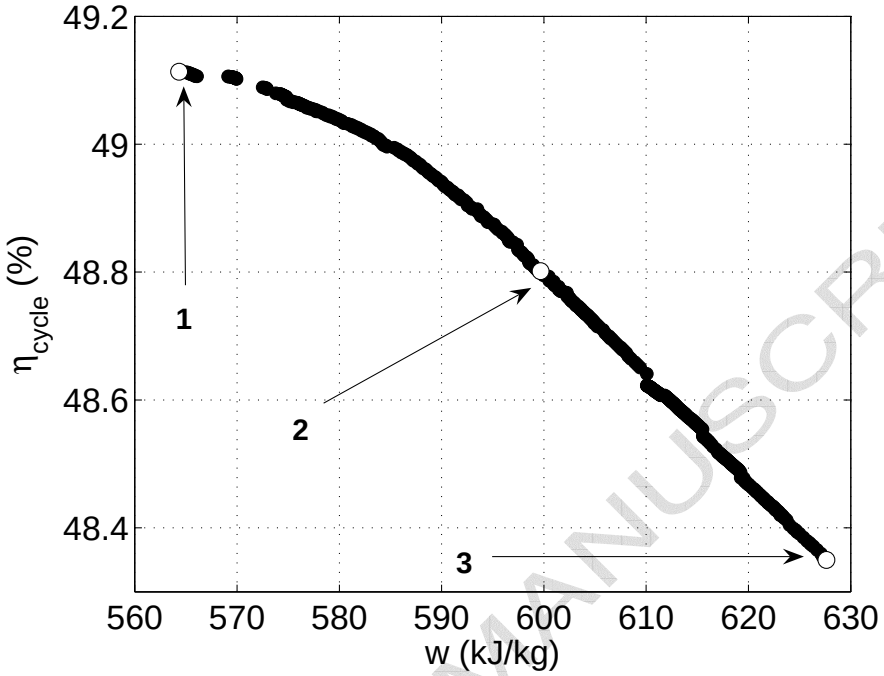

Fig. 7. Selected STIG systems from Pareto-optimal set for cooling optimisation

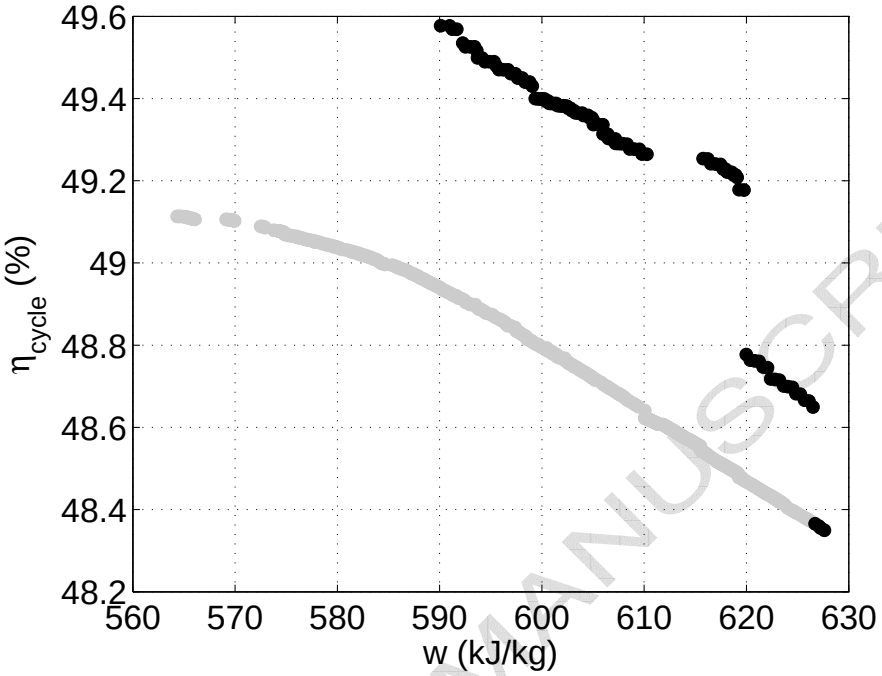

Fig. 8. Comparison of the cooling optimised STIG Pareto-optimal set (black dots) and the original Pareto-optimal set (gray dots)

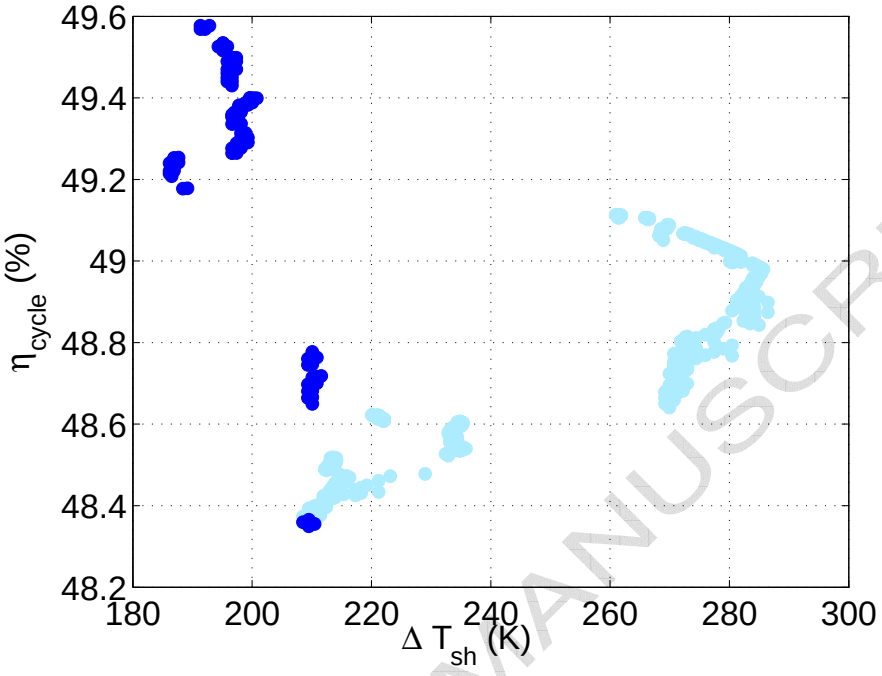

Fig. 9. Efficiency against superheat for the cooling optimised STIG Pareto-optimal set (dark dots) and the original Pareto-optimal set (light dots)

List of Tables

Parameter	Description	Value
n_{stm}	Size of the STM	10
$n_{regions}$	Search space split into $N \times n_{regions}$ regions in the LTM	4
n_{sample}	Number of points randomly sampled at each move	6
$i_{intensify}$	Number of iterations after a successful addition to the MTM at which an intensification move is performed	25
$i_{diversify}$	Number of iterations after a successful addition to the MTM at which a diversification move is performed	45
i_{reduce}	Number of iterations after a successful addition to the MTM at which a step-size reduction move is performed	90
h	Initial step-size (as a percentage of the range of each variable)	8%
δh	Step-size reduction factor	0.5

Table 1
Optimiser parameters

	Coolant Flow						
	HP1	**HP2**	**IP1**	**IP2**	**D1**	**D2**	**D3**
A	HP5	HP4	HP3	HP2	HP3	HP1	LP7
B	HP5	HP5	HP3	HP3	HP3	HP1	HP1
C	SAT	SAT	HP3	HP3	HP3	HP1	LP7
D	SAT	SAT	HP3	HP3	HP3	HP1	HP1

Table 2
Coolant bleed point configuration for each HAT specification

	Net Work Output(kJ/kg)	Heat Input(kJ/kg)	Total Coolant/Compressor Inlet Ratio m_c/m_g (%)	Overall Efficiency η_{ov}(%)
A	584.27	1193.59	15.068	48.951
	Ratio of values relative to Case A			$\eta_{ov} - \eta_{ov,A}$
B	0.993	0.998	1.028	-0.258
C	1.009	1.013	0.881	-0.184
D	1.008	1.014	0.882	-0.259

Table 3
Overall performance figures for HAT cycle

	Coolant Flow						
	HP1	**HP2**	**IP1**	**IP2**	**D1**	**D2**	**D3**
A	HP6	HP4	HP3	HP2	HP3	HP1	LP7
B	HP6	HP4	HP3	HP3	HP3	HP3	HP3
C	ST	ST	HP3	HP2	HP3	HP1	LP7
D	ST	ST	HP3	HP2	HP3	HP2	HP2
E	ST	ST	ST	ST	HP3	HP1	HP1
F	SA	SA	HP3	HP2	HP3	HP1	LP7
G	SA	SA	HP3	HP2	HP3	HP2	HP2

Table 4
Coolant bleed point configuration for STIG cycle with 50% steam utilisation

	Coolant Flow						
	HP1	**HP2**	**IP1**	**IP2**	**D1**	**D2**	**D3**
A	HP6	HP4	HP3	HP2	HP3	HP1	LP8
B	HP6	HP4	HP3	HP3	HP3	HP3	HP3
C	ST	ST	HP3	HP3	HP6	HP6	LP8
D	ST	ST	HP3	HP2	HP3	HP2	HP2
E	ST	ST	ST	ST	HP3	HP2	LP8
F	SA	SA	HP3	HP2	HP3	HP2	LP8
G	SA	SA	HP3	HP2	HP3	HP2	HP2

Table 5
Coolant bleed point configuration for STIG cycle with 100% steam utilisation

	Net Work Output(kJ/kg)	Heat Input(kJ/kg)	Total Coolant/Compressor Inlet Ratio m_c/m_g (%)	Overall Efficiency η_{ov}(%)
A	474.94	1136.52	16.727	41.789
	Ratio of values relative to Case A			$\eta_{ov} - \eta_{ov,A}$
B	0.995	1.000	1.008	-0.201
C	1.077	1.044	0.763	1.359
D	1.076	1.045	0.763	1.267
E	1.096	1.054	0.704	1.702
F	0.981	0.988	1.005	-0.307
G	0.979	0.988	1.005	-0.402

Table 6
Overall performance figures for STIG cycle with 50% steam utilisation

	Net Work Output(kJ/kg)	Heat Input(kJ/kg)	Total Coolant/Compressor Inlet Ratio m_c/m_g (%)	Overall Efficiency η_{ov}(%)
A	708.93	1473.93	21.465	48.098
	Ratio of values relative to Case A			$\eta_{ov} - \eta_{ov,A}$
B	0.997	1.000	1.010	-0.127
C	0.989	0.987	0.719	0.069
D	0.989	0.988	0.719	0.032
E	0.958	1.054	0.591	-0.268
F	0.981	0.985	0.933	-0.205
G	0.981	0.986	0.934	-0.242

Table 7
Overall performance figures for STIG cycle with 100% steam utilisation

	Coolant destination							$\eta_{ov} - \eta_{ov,ref}$ (%)	Coolant savings (%)
	HP1	**HP2**	**IP1**	**IP2**	**D1**	**D2**	**D3**		
	Coolant source								
REF	HP6	HP6	HP3	HP3	HP6	HP6	HP3	-	-
1	HP6	HP6	HP3	HP3	HP6	HP6	HP3	0.0	0.0
2	HP6	HP5	HP3	HP1	HP6	HP6	HP3	0.192	3.1
3	HP6	HP4	HP3	HP3	HP6	HP6	HP3	0.252	4.3
TS	HP5/SAT/AC	HP4	HP3	HP1	HP6	HP6	HP3	0.3-0.5	5.5-14

Table 8
HAT cooling optimisation of the Pareto-optimal set

	Coolant destination							$\eta_{ov} - \eta_{ov,ref}$ (%)	Coolant savings (%)
	HP1	**HP2**	**IP1**	**IP2**	**D1**	**D2**	**D3**		
	Coolant source								
REF	HP6	HP6	HP3	HP3	HP6	HP6	LP8	-	-
1	HP6	HP6	HP3	HP3	HP6	HP6	LP8	0.0	0.0
2	HP6	HP6	HP3	HP2	HP6	HP6	LP8	0.05	0.7
3	SA	HP6	HP3	HP3	HP6	HP6	LP8	0.054	5.5
TS	SA/ST/HP6	ST/HP6	HP3	HP3	HP6	HP6	LP8	0.3-0.5	15-35

Table 9
STIG cooling optimisation of the Pareto-optimal set

BASIC GAS TURBINE COMPONENTS						
			Stage 1		Stage 2	
COMPRESSOR		**COOLING**	stator	rotor	stator	rotor
Pressure ratio (β)	20.0	Max metal temperature, $T_{m,max}$ (K)	1075	1025	1025	1025
Mass flow-rate, m_g (kg/s)	100.0	Combustion pattern factor, K_{comb}	0.5	0.35	0.20	0.15
Pressure split (Π)	0.5	Swirl factor, K_{swirl}		0.5		
Stages (IP/HP)	8/6	Internal cooling efficiency, $\eta_{c,int}$		0.7		
Polytropic efficiency, η_p (IP/HP)	0.9/0.9	Film cooling effectiveness, ε_{film}		0.3		
Mechanical efficiency, η_{mech} (%)	99.0	Metal Biot number, Bi_m		0.2		
COMBUSTOR		TBC Biot number, Bi_{tbc}		0.3		
TIT (K)	1573	Gas Mach Number, $M_{g,x}$		0.8		
Gas pressure loss, Δp_g (%)	5.0	Coolant injection angle, $\phi_{injection}$ (°)		30.0		
TURBINE		Chord ratio		0.03		
Stages (IP/HP/FPT)	1/1/4	Area ratio		7.74		
Polytropic efficiency, η_p (HP)	0.87	Pitch/Chord ratio		0.6		
Polytropic efficiency, η_p (IP)	0.87	Opening/Pitch ratio		0.5		
Polytropic efficiency, η_p (FPT)	0.91	Stagger angle		30.0		
Stage load factor, ψ	1.4	Metal thickness (m)		0.002		
EXHAUST		Metal conductivity (W/m)		34.62		
Gas pressure loss, Δp_g (%)	5.0	TBC thickness (m)		0.00025		
GENERATOR		TBC conductivity (W/m)		0.7		
Gearing losses (%)	0.7	Momentum ratio		0.6		
Electrical losses (%)	1.0		HPT	IPT	FPT	
		Disk flow fraction	0.02	0.01	0.01	

Table 10
System reference parameters for basic GT

HUMID CYCLE COMPONENTS		
	HAT	STIG
COMPRESSOR		
Pressure ratio (β)	20	20
INTERCOOLER/AFTERCOOLER		
Effectiveness, ε	0.85	-
Gas pressure loss, Δp_g (%)	6.0	-
ECONOMISER		
Effectiveness, ε	0.85	-
Gas pressure loss, Δp_g (%)	3.0	-
RECUPERATOR		-
Effectiveness, ε	0.95	-
Gas pressure loss (hot side), $\Delta p_{g,h}$ (%)	8.5	-
Gas pressure loss (cold side), $\Delta p_{g,c}$ (%)	6.0	-
SATURATOR		
Pinch temperature difference, ΔT_{pinch} (K)	5.5	-
WATER CIRCUIT		
Water supply temperature, T_{w0} (K)	288.15	288.15
Water supply pressure, p_{w1} (bar)	p_{g2} + 1.0	p_{g2} + 10.0
Flow fraction into intercooler, $\bar{m}_{ic}$ (-)	0.5	-
Flow fraction into economiser, $\bar{m}_{eco}$ (-)	0.5	-
Saturator water/gas ratio, $\bar{m}_{sat}$ ($\mathrm{kg}_w/\mathrm{kg}_{g,in}$)	1.268	-
STEAM GENERATOR		
Pinch temperature difference, ΔT_{pinch} (K)	-	10.0
Amount of superheat, ΔT_{sh} (K)	-	150.0
Gas pressure loss, Δp_g (%)	-	3.5
Water pressure loss, Δp_w (%)	-	2.5
Minimum exhaust temperature, $T_{exh,min}$ (K)	373.15	373.15
Economiser heat transfer coeff, U_{eco} ($\mathrm{W/m^2}$)	50.0	50.0
Evaporator heat transfer coeff, U_{ev} ($\mathrm{W/m^2}$)	-	40.0
Superheater heat transfer coeff, U_{sh} ($\mathrm{W/m^2}$)	-	40.0
STEAM INJECTION		
Steam utilisation (% of steam generated)	-	50.0

Table 11
System reference parameters for humid GT